PROCEEDINGS OF SPIE

SPIEDigitalLibrary.org/conference-proceedings-of-spie

Ultraviolet hyperspectral interferometric microscopy

Robles, Francisco

Francisco E. Robles, "Ultraviolet hyperspectral interferometric microscopy," Proc. SPIE 10888, Biophysics, Biology and Biophotonics IV: the Crossroads, 108880A (4 March 2019); doi: 10.1117/12.2511967



Event: SPIE BiOS, 2019, San Francisco, California, United States

Ultraviolet hyperspectral interferometric microscopy

Francisco E. Robles^{1,*}

¹Wallace H. Coulter Department of Biomedical Engineering, Georgia Institute of Technology and Emory University, Atlanta, Georgia 30332, USA

ABSTRACT

Ultraviolet (UV) spectroscopy is a powerful tool for quantitative biochemical analysis, but its application to molecular imaging and microscopy has been limited. Here we describe our recent work on ultraviolet hyperspectral interferometric (UHI) microscopy, which leverages coherent detection of optical fields to overcome significant challenges associated with UV spectroscopy when applied to molecular imaging. We demonstrate that this method enables quantitative spectral analysis of important endogenous biomolecules with subcellular spatial resolution and sensitivity to nanometer-scaled structures for label-free molecular imaging of live cells.

1. INTRODUCTION

Ultraviolet hyperspectral interferometric (UHI) microscopy¹ is a recently developed molecular imaging technique that retrieves wideband, high-resolution spectral information of the wavelength-dependent real part of the refractive index (i.e., dispersion), and the total attenuation coefficient of biological samples in the deep-ultraviolet (UV) spectral region. This method enables highly sensitive, label-free molecular imaging with sensitivity to various dispersion-causing and absorptive biomolecules that play an important role in diseases, including cancer. UHI also provides insight into structure of biological samples by yielding quantitative phase maps with subcellular spatial resolution and nanometer-scaled sensitivity. In this work, we give a detailed description of the UHI system, signal processing methods, and demonstrate its ability to quantify the dispersive and absorptive properties of biological samples in the deep-UV spectral region (240-450 nm). We also show dispersion, absorption, and quantitative phase data from red blood cells, as well as nucleated cells (e.g., granulocytes). Finally, we assess the deep-UV dispersion and absorptive properties of important biomolecules (e.g., DNA, NADH, FAD, collagen, cytochrome C, and hemoglobin) ², and discuss the implications of this work.

Keywords: Deep UV microscopy, quantitative phase imaging, spectroscopy, label-free molecular imaging

2. SYSTEM AND METHODS

The UHI system (Fig. 1) consists of an incoherent broadband laser-driven plasma light source (EQ-99X LDLS, Energetiq Technology) along with a modified Mach-Zehnder interferometry configuration. The output light from the broadband source is collimated through a set of off-axis paraboloid mirrors and relayed via the 4-f optical configuration. The interferometer itself is also configured as a 4-f interferometer to enable coherent detection using a partially incoherent, broadband light source^{3,4}. Effectively, this geometry spatially separates the modes of the source on the sample, thus each mutually coherent area illuminates a diffraction limited spot on the sample which is then relayed onto the camera for interferometric detection. For imaging, we use 40X (NA 0.5), UV microscope objectives and achieve an average spatial resolution of ~300 nm. Data are collected with an imaging spectrometer equipped with a high-speed back-illuminated sCMOS camera with the integration time set to 100 ms. Information is recorded as a function of one spatial dimension along the rows of the camera, and spectrum across the columns of the camera. Then, the sample is translated across the orthogonal spatial dimension to recover a hyperspectral data cube.

After acquiring an interferogram, which contains the signal as a function of wavelength and one spatial dimension, we interpolate the data to wavenumber ($k=2\pi/\lambda$) and apply a 2-D Fast Fourier transform (FFT). The interferometric signal of interest is filtered (using a Butterworth filter) and shifted to DC to demodulate the interferometric signal, similar to holographic processing methods^{5,6}. Then the inverse transform is taken which gives the complex field, i.e., the broadband amplitude and phase spectra of the field along one spatial dimension. This process is repeated for each 2D data set (complex spectrum and one spatial dimension) to construct a 3D complex hyperspectral data cube.

robles@gatech.edu

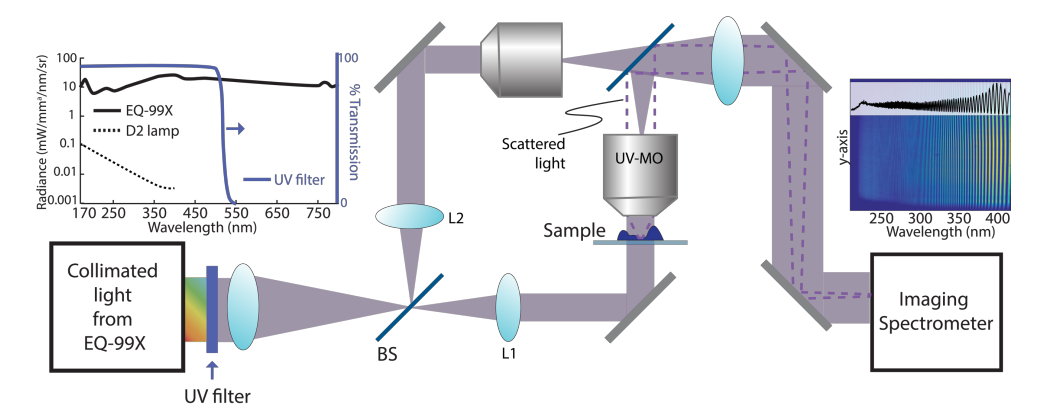


Figure 1. The UHI microscopy system. The light source is a broadband plasma driven lamp that is collimated and sent into a Mach-Zehnder interferometry. Spectrum of the source output light is depicted in the left inset. The beam is split into reference and sample beams via the first beam splitter (BS) and collimated using L1 and L2 lenses. The imaging is performed using UV objectives (UV-MO) and the interferometric data (a sample image is shown in the right inset) is recorded by the imaging spectrometer. Taken from Ref¹.

The measured complex field is used to mitigate the effects of chromatic aberration in the UV range. To this end, the complex field is refocused at all wavelengths using Fresnel propagation⁷ where the wavefronts are digitally propagated according to the chromatic aberration-induced focal length shift of the UV objective. This process yields focused amplitude and phase images throughout the imaging spectral range (e.g., 240 nm-450 nm). The phase information yields a resolution of 1.4 nm measured from the standard deviation of the phase map in a background region.

The signal at each pixel of the sample after removing the DC and complex conjugate term (as described above) can be expressed in complex form as^{3,8},

$$\tilde{I}(\lambda) = I_0(\lambda) \cdot e^{-(\mu_a(\lambda) + \mu_s(\lambda))L} \cdot e^{-ikL(n(\lambda))}$$
(1)

Here I_0 is the initial intensity which depends on the source, the next term describes attenuation, including absorption (μ_a) and scattering (μ_a) , and the last term contain the refractive index (RI, n) information which depends on wavelength (this is know as dispersion). Also, L is the thickness of the sample, $k = 2\pi/\lambda$ is wavenumber and λ is the wavelength of light. Thus, the recovered signal yields access to both the attenuation and dispersive (changes in RI) properties.

For the spectroscopic results presented below, we further process the signals to yield concentration independent quantities. For solution samples, scattering is negligible, thus the attenuation signal can be processed to yield the molar extinction coefficient, ε :

$$-ln\left(\frac{|\tilde{I}(\lambda)|}{|I_0(\lambda)|}\right) = \mu_a(\lambda)L\tag{2}$$

$$\varepsilon(\lambda) = \mu_a(\lambda) M / (c \cdot ln(10)) \tag{3}$$

Where M is the molecular weight and c is the concentration. For the RI, we convert the signal into B, the refractive index increments—a concentration independent measurement—defined by,

$$n(\lambda) = n_{medium}(\lambda) + B(\lambda)c$$

With a measurement of the sample and the medium for reference, the measured phase signal in Eq. 1 yields $B \cdot c$.

3. RESULTS

3.1 Spectroscopy results.

Here we present the absorptive and dispersive properties of various important endogenous biomolecules². These samples were diluted in water and placed inside a flow cell to maintain a constant sample thickness (note that we are sensitive to nanometer scale differences). A measurement with the solvent (water) was also taken and used as reference.

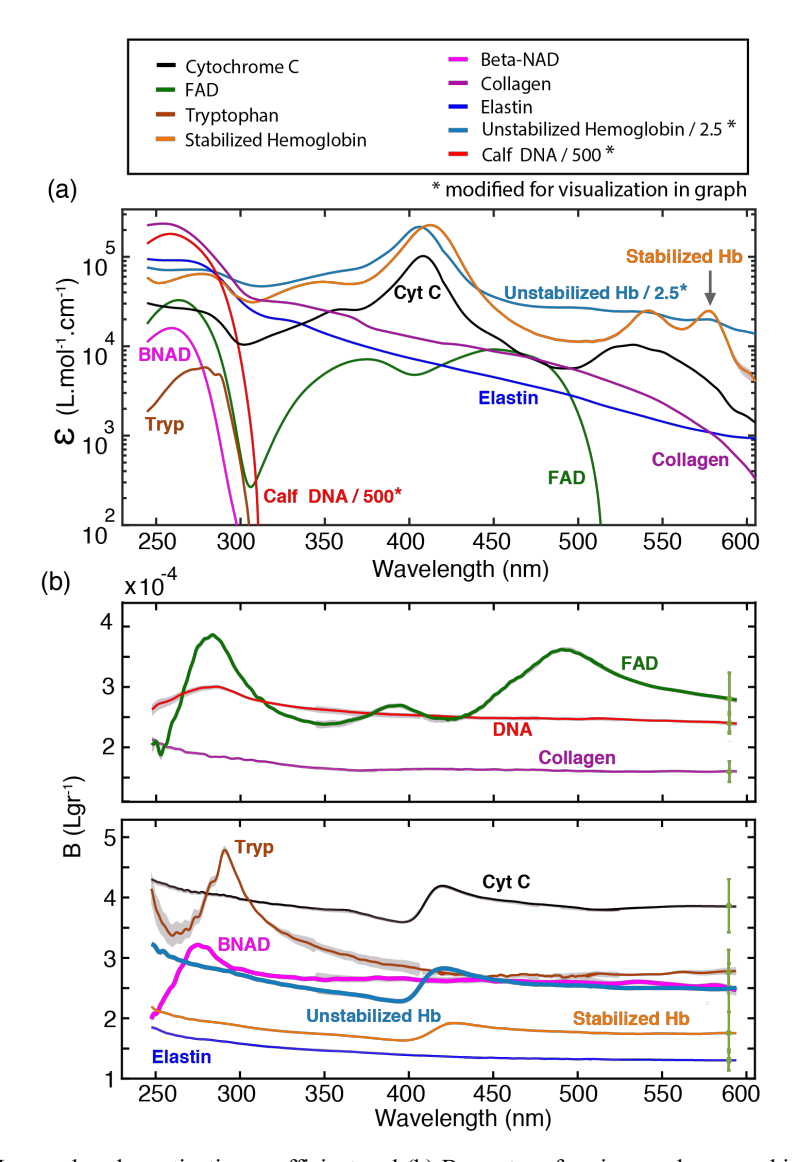


Fig. 2 (a) Measured molar extinction coefficient and (b) B-spectra of various endogenous biomolecules. To plot all the graphs in a single frame, we have divided the Unstabilized Hemoglobin data by 2.5 and Calf DNA data by 500 as stated in the figure. B graphs are split for clarity as some curves overlap significantly in certain regions. Taken from Ref².

There a number of interesting features in the presented spectra in Fig 2. For the extinction, most biomolecules show strong absorption around 260 and 280 nm which corresponds to the absorption peaks of nucleic acid and proteins. For hemoglobin and cytochrome, we can observe the strong Soret band around 415nm. Collagen and elastin show a featureless spectrum that is monotonically decreasing. On the dispersion plot, the characteristic 'S-shape' can be observed at regions corresponding to the absorption peaks. FAD shows a surprising structured spectrum with resonances much more variable than any other type of molecule, including Hb which has more prominent absorption peaks. These results were recently published in Ref. ² and raw data of the spectra can be found in the supplemental material.

3.2 Red blood cells and neutrophil imaging with UHI

Figure 3 shows the UHI microscopy results of a red blood cell¹. Here we can clearly see the typical biconcave shape of an RBC in Fig 3a. Figure 3d shows both the original, out-of-focus image due to chromatic aberrations and the corrected intensity image. The absorption and dispersion spectra are also shown. These results are also compared to a solution of Hb to verify that we can extract the expected properties from a single cell.

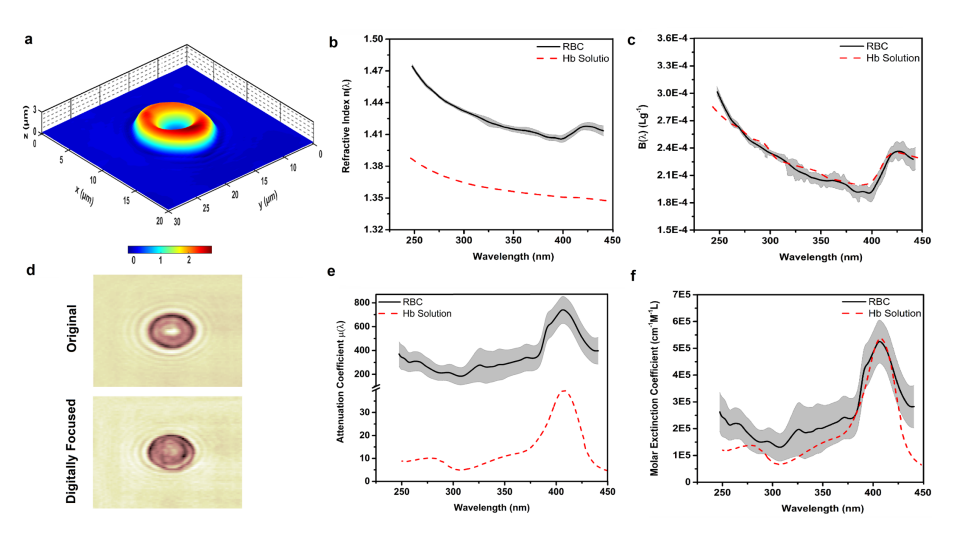


Figure 3. UHI microscopy of a live RBC. (a) Topological map of estimated thickness for an isolated human RBC (axes in μ m). (b) Refractive index for RBC (black line) within one standard deviation range (gray area) and 2 g/dL Hb solution (dashed red line). (c)Real refractive increment (B) spectra for the imaged RBC and Hb solution. (d) Amplitude maps of an imaged RBC before and after digital refocusing at 390nm. (e) Attenuation coefficient spectra for RBC (black line) within its standard deviation range (gray area) and Hb solution (dashed red line). (f) Molar extinction coefficient spectra for the RBC and Hb solution. Taken from Ref¹

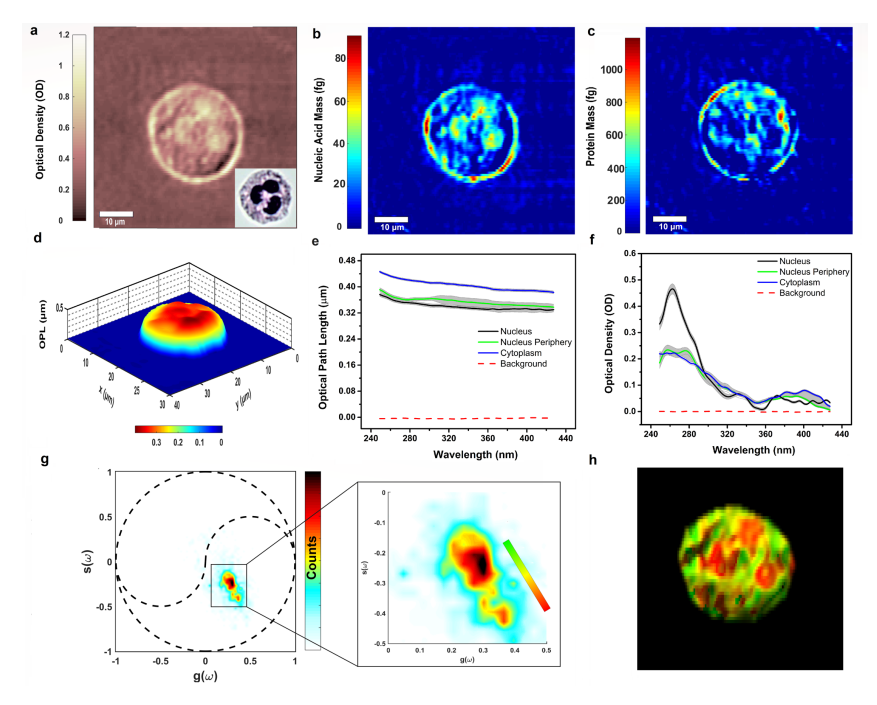


Figure 4. UHI microscopy of a live neutrophil. (a) Optical density (OD) map of an *unstained*, isolated human neutrophil at 260nm wavelength with inset depicting a bright-field microscopy image of the same neutrophil *after Giemsa staining*. (b) Nucleic acid mass map of a neutrophil with an average mass of 23.81 fg within cell. (c) Protein mass map of a neutrophil with an average mass of 273.65 fg within cell. (d) OPL map of a neutrophil at 260 nm. (e) OPL spectra averaged over cell nucleus, nucleus periphery, and cytoplasm. (f) Optical density spectra extracted from cell nucleus, nucleus periphery, and cytoplasm. (g) Phasor space representation of the attenuation spectra obtained from the imaged neutrophil, bounded by the unit circle as well as the universal semicircles (dashed black lines) (h) Molecular image obtained by color coding the phasor space clusters based on the colorbar shown in Fig. 2(g) inset. Taken from Ref¹

Figure 4 shows the results for a neutrophil. These types of cells have a polymorphonuclear structure and contain granules, providing a more complex structure compared to RBCs which are basically homogeneous inside. The spectral results in Fig 4f and 4e show the clear absorptive properties from nucleic acid and proteins, but interestingly, the dispersive properties lack the expected structure. From Fig 2 above, it is observed that DNA does not show a strong dispersive signature, thus the relative featureless spectrum from the nuclei of the neutrophil is not a complete surprise, particularly if other molecules are present which further distort the spectrum by broadening any dispersive features. In Fig 4g we use an unsupervised method of spectral analysis called phasor analysis. Here we see that two main clusters are formed corresponding to the nuclei and cytoplasm. However, the later cluster has a broad structure which signifies the presence of many subtle differences in spectrum, likely due to the granules which contain myeloperoxidase. Here scattering may be adding additional heterogeneity to the spectrum.

4. CONCLUSION

UHI microscopy¹ offers unique opportunities to leverage the biochemical specificity of UV spectroscopy for label-free molecular imaging¹⁰. Here we have presented an analysis of the absorptive and dispersive properties of important endogenous biomolecules that play an important role in cell and tissue function, and shown preliminary results from blood cells. This method has significant potential to provide detailed insight into biochemical and structural changes associated with, for example, disease progression and staging¹¹¹-¹⁵ or more dynamic processes like cell motility and proliferation¹⁶. We expect UHI microscopy to become an important tool for a variety of biomedical applications including characterization and phenotyping of cells and thin tissue biopsy samples.

5. ACKNOWLEDGMENTS

I gratefully acknowledge the funding sources for this work: National Science Foundation (NSF CBET CAREER 1752011); Burroughs Welcome Fund (CASI BWF1014540); Galloway Foundation and Integrated Cancer Research Center, Georgia Institute of Technology.

7. REFERENCES

- 1. Ojaghi, A., Fay, M. E., Lam, W. A. & Robles, F. E. Ultraviolet Hyperspectral Interferometric Microscopy. *Sci. Rep.* **8**, 1–6 (2018).
- 2. Soltani, S., Ojaghi, A. & Robles, F. E. Deep UV dispersion and absorption spectroscopy of biomolecules. *Biomedical Optics Express* 1–13 (2019). doi:10.1364/OA License v1
- 3. Robles, F. E., Satterwhite, L. L. & Wax, A. Nonlinear phase dispersion spectroscopy. *Optics Letters* **36**, 4665–4667 (2011).
- 4. Graf, R., Brown, W. & Wax, A. Parallel frequency-domain optical coherence tomography scatter-mode imaging of the hamster cheek pouch using a thermal light source. *Optics Letters* **33**, 1285–1287 (2008).
- 5. Wang, S., Xue, L., Lai, J. & Li, Z. An improved phase retrieval method based on Hilbert transform in interferometric microscopy. *Optik International Journal for Light and Electron Optics* **124**, 1897–1901 (2013).
- 6. Mir, M., Bhaduri, B., Wang, R., Zhu, R. & Popescu, G. *Quantitative Phase Imaging. Progress in Optics* 57, 133–217 (Elsevier Inc., 2012).
- 7. Goodman, J. W. *Introduction to Fourier optics*. (2005). doi:10.1234/12345678
- 8. Robles, F. E. & Wax, A. Separating the scattering and absorption coefficients using the real and imaginary parts of the refractive index with low-coherence interferometry. *Optics Letters* **35**, 2843–2845 (2010).
- 9. Robles, F. E., Wilson, J. W., Fischer, M. C. & Warren, W. S. Phasor analysis for nonlinear pump-probe microscopy. *Opt. Express* **20**, 17082 (2012).
- Zeskind, B. J., Jordan, C. D., Timp, W., Trapani, L., Waller, G., Horodincu, V., Ehrlich, D. J. & Matsudaira,
 P. Nucleic acid and protein mass mapping by live-cell deep-ultraviolet microscopy. *NATURE METHODS* 4, 567–569 (2007).
- 11. Robles, F. E., Deb, S., Wilson, J. W., Gainey, C. S., Selim, M. A., Mosca, P. J., Tyler, D. S., Fischer, M. C. & Warren, W. S. Pump-probe imaging of pigmented cutaneous melanoma primary lesions gives insight into metastatic potential. *Biomedical Optics Express* **6**, 3631–3645 (2015).
- 12. Robles, F. E., Wilson, J. W. & Warren, W. S. Quantifying melanin spatial distribution using pump-probe microscopy and a 2-D morphological autocorrelation transformation for melanoma diagnosis. *J Biomed Opt* **18**, 120502 (2013).

- 13. Sridharan, S., Sridharan, S., Macias, V., Macias, V., Tangella, K., Tangella, K., Kajdacsy-Balla, A., Kajdacsy-Balla, A. & Popescu, G. Prediction of prostate cancer recurrence using quantitative phase imaging. *Sci. Rep.* **5**, 9976 (2015).
- 14. Uttam, S., Pham, H. V., LaFace, J., Leibowitz, B., Yu, J., Brand, R. E., Hartman, D. J. & Liu, Y. Early Prediction of Cancer Progression by Depth-Resolved Nanoscale Mapping of Nuclear Architecture from Unstained Tissue Specimens. *Cancer Res* **75**, 4718–4727 (2015).
- 15. Robles, F. E., Deb, S., Fischer, M. C., Warren, W. S. & Selim, M. A. Label-Free Imaging of Female Genital Tract Melanocytic Lesions With Pump-Probe Microscopy. *Journal of Lower Genital Tract Disease* **21**, 137–144 (2017).
- 16. Park, Y., Depeursinge, C. & Popescu, G. Quantitative phase imaging in biomedicine. *Nature Photon* **12**, 1–12 (2018).